Initial Evolution of Passivation Layers in Non-Aqueous Aluminium Batteries

OPEN ACCESS

Initial Evolution of Passivation Layers in Non-Aqueous Aluminium Batteries

Journal of The Electrochemical Society, 2023 **170** 030512

Initial Evolution of Passivation Layers in Non-Aqueous Aluminium Batteries

Laura C. Loaiza,[1,z] Niklas Lindahl,[2] and Patrik Johansson[1,3]

[1]*Department of Physics, Chalmers University of Technology, SE-41296 Göteborg, Sweden*
[2]*Department of Physics, University of Gothenburg, SE-412 96 Göteborg, Sweden*
[3]*ALISTORE-European Research Institute, FR CNRS 3104, Hub de l'Energie, 15 Rue [3]Baudelocque, 80039 Amiens, France*

Aluminium batteries (AlBs) have gathered considerable attention, primarily due to the high capacity, the low cost, the large abundance in the Earth's crust, and the recyclability of the Al metal anode. However, several hurdles must be surpassed to make AlBs a feasible energy storage technology and two of them are interconnected; the presence of an ionic and electronically insulating native oxide layer on the Al metal anode that calls for special non-aqueous, most often ionic liquid based acidic electrolytes, to enable reversible plating and stripping of Al. We here find the passivation layer initially formed in contact with an ionic liquid electrolyte (ILE) to have a porous and very complex nature, i.e. an outer inorganic/organic layer and an inner oxide-rich layer. Furthermore, it grows under open circuit voltage conditions by simultaneous dissolution and re-deposition of dissolved products, while during galvanostatic cycling this is exacerbated by an electrochemical etching that causes pitting corrosion of the Al metal itself. All of this leads to unstable interfaces being formed and the co-existence of several species at the Al metal anode surface, of which a proper understanding and mitigation are crucial to make AlBs a reality.
 [DOI: 10.1149/1945-7111/acb108]

Manuscript submitted September 1, 2022; revised manuscript received December 12, 2022. Published March 9, 2023. *This paper is part of the JES Focus Issue on Selected Papers from IMLB 2022.*

Supplementary material for this article is available online

Aluminium (Al) is an attractive metal for battery application due to its low cost, its large abundance in the Earth's crust, a mature production process, and not the least its well-developed recyclability —less energy-intense than the extraction.[1] However, foremost it is due to its ability as a metal anode to release three electrons that results in a very high theoretical volumetric capacity 8046 mAh cm^{-3} (vs 2062 mAh cm^{-3} for lithium metal) and a likewise vast gravimetric capacity of 2980 mAh g^{-1}.[2] In addition, it can double as current collector (CC), which further lowers the AlB cell weight.[3] Aluminum batteries (AlBs) are made using either aqueous or non-aqueous electrolytes with the Al-oxide native passivation layer as a common major challenge, due to its ionic and electronic insulating nature. For aqueous AlBs it hinders the reversible plating and stripping of Al as it shifts the hydrogen evolution reaction (HER) potential, rendering the HER the main cathodic reaction.[4] One approach used is to engineer an artificial solid electrolyte interphase (SEI) layer to replace the native passivation layer and hinder its reformation,[5] but the efficiency of this strategy is debated.[4]

Turning to non-aqueous AlBs, several ionic liquid based electrolytes (ILEs) have been applied and explored,[6–8] such as AlCl3: EMIMCl which allows reversible plating and stripping of Al.[9] This ability is ultimately dependent on the presence of $Al2Cl7^-$ (Eq. 1), which formation in turn depends on the molar ratio (r) of AlCl3: EMIMCl; only for r>1 $Al2Cl7^-$ is formed and the electrolyte is a Lewis acid.[2,10,11] This is a major concern as the reactivity of all cell components towards the ILE must be addressed, e.g. alternative cathode CCs are needed as stainless steel (SS), Cu, and Al CCs will corrode.[12]

$$4Al_2Cl_7^- + 3e^- \rightarrow Al + 7AlCl_4^- \quad [1]$$

On the other hand, the Al-oxide native passivation layer offers some protection to ILE induced corrosion, but it also hinders the Al-ion transfer and redox reactions.[13] Yet, this native passivation layer does not totally withstand the acidic conditions and eventually dissolves into the ILE. This also influences the Al plating and stripping and possibly pushes it towards detrimental dendrite formation. In the literature, Chen et al.[14] concluded that the Al-oxide native passivation layer prevents Al metal electrode disintegration by decreasing the nucleation sites, and thereby controls the dendrite growth, while Long et al.[13] showed that it dissolves in the ILE and is replaced by an SEI-layer rich in Cl and O species and that dendrite formation can be reduced by using a porous Al structure. Moreover, Lee et al.[15] studied the morphological changes on Al metal as a function of dipping time in the ILE and revealed local attacks followed by the formation a new oxide layer, with a specific lattice plane and craterlike surface. Overall, this shows that the roles of the Al-oxide native and ILE-derived passivation layers and their evolution in an AlB are far from fully understood, but seem to have a profound impact on the electrochemical performance, in aqueous[16] and non-aqueous AlBs alike.[14] Additionally, the very development of alternative and non-corrosive non-aqueous AlB electrolytes has been impeded by the need of pre-treatments and/or some amount of corrosion in order to guarantee proper electrolyte to Al metal anode contact.[17]

To track the initial evolution of these passivation layers at the Al metal anode surface, in contact with a non-aqueous acidic ILE, under both open circuit voltage (OCV) and galvanostatic cycling (GC) conditions, we here use a combination of potentiostatic electrochemical impedance spectroscopy (PEIS), X-ray photoelectron spectroscopy (XPS), and scanning electron microscopy (SEM) tools and data. The goal is to shed light on their compositions and roles played in the functionality of AIBs, to finally enable to rationally improve AlB performance.

Experimental

Al|Al (99.997%, 0.1 mm, Alfa Aesar) symmetric cells (**Cells 1–9**) were assembled inside an argon filled glove box using two-terminal Swagelok-type cells (Fig. S1), with tungsten (W) foil (99.95%, 0.1 mm, Alfa Aesar) as CCs, a glass fiber separator (Whatman GF/C), and 30 μl of $AlCl_3$: EMIMCl 1.5:1 (Sigma Aldrich) as electrolyte.

PEIS was carried out in the frequency range of 4 mHz to 1 MHz, with an excitation voltage of 10 mV. The GC was performed with a constant current density of 0.25 mA cm^{-2} applied for a predetermined time. **Cells 1**, **2** and **3** were left at OCV for 60 h, with PEIS performed each 1–2 h. Following this, GC combined with PEIS was performed after 5, 15, 20, 60, 120, 240 and 360 min. **Cells**

[z]E-mail: laura.loaiza@chalmers.se

4–5 did not undergo the OCV step and the GC was performed right after cell assembly. For all the cells, the PEIS data were fitted to equivalent circuits (ECs) using the Zview Scribner software (**SI, note 1**). All electrochemical measurements were performed using a Bio-Logic VMP3 potentiostat.

The electrodes of **Cells 6–9** were recovered after 5 (**Cell 6**) and 60 h (**Cell 7**) OCV and after 60 h OCV + 15 (**Cell 8**) and 360 min GC (**Cell 9**), respectively. These cells were disassembled inside the glove box and the electrodes were washed with a mixture of 1:1 dimethoxyethane:tetrahydrofuran (DME:THF), to remove any traces of the ILE, the excess of solvent was evaporated under vacuum. The recovered electrodes were studied by SEM with a field emission Supra 35 VP Carl Zeiss microscope at 10 kV acceleration voltage and XPS using a PHI VersaProbeIII system. In order to avoid exposure to ambient atmosphere, inert transfer from the glove box to the XPS chamber was made using a vacuum transfer vessel. The XPS X-ray source was monochromatic Al Kα (1486.7 eV) and the concentric hemispherical analyzer was positioned at 45° angle from the sample normal. Energies were shifted to set the position of the metallic Al2p-peak to 72.6 eV. The area of measurement was *ca.* 500 × 500 μm^2. Furthermore, depth-profiling was performed by Ar-sputtering to plasma-etch the surface to analyze the passivation layers' compositions as a function of depth. The 1st etch was for 2 min at 500 V, over an area of 2 × 2 mm^2 (calibrated to give 1.0 nm etching-depth in Ta-oxide); the 2nd etch was for 2 min at 1 kV, over an area of 2 × 2 mm^2 (calibrated to give 2.1 nm etching-depth in Ta-oxide); and the 3rd etch was also for 2 min at 1 kV over an area of 2 × 2 mm^2.

Results and Discussion

First, we report on the Al|Al symmetric cells, under OCV conditions (**Cells 1–3, 6, 7**) as well as after/during GC (**Cells 1–5, 8, 9**), and for both we describe all the changes observed by all the various characterization techniques employed. This is followed by a concerted discussion based on different scenarios where the initial formation and the subsequent evolution of the passivation layers are targeted.

Passivation layer formation under OCV conditions.—For **Cells 1–3**, the resistance increases with time and the profile of the spectra changes; in the Nyquist plots (Figs. 1a, S2a-S3a), two partly overlapping semicircles can be detected, a smaller one at high frequency and a larger one at low frequency, more easily seen in the Bode plot (Figs. 1b, S2b-S3b). Therein at least two peaks are observed, corresponding to different time-constants; one at high frequency with a shoulder and another one at low frequency, which gradually shifts towards lower frequencies. The phase angle for the former is ≈ −70°, indicating a capacitive behavior and thus a passivation layer. Indeed, as our Al electrodes are used without any further preparation, the Al-oxide native passivation layer is naturally present. By a closer look, this peak has two time-constants of similar magnitude, corresponding to processes taking place at the same time and/or being of a very similar nature. Possibly this is due to the oxide-rich passivation layer and the formation of another passivation layer (inorganic/organic), the latter derived from decomposition products of the ILE, in analogy to the observations by Long et al.[13] The second peak at low frequencies then corresponds to the processes taking place at the metal/passivation layers interface and as it shifts to lower frequencies, a more resistive process. This peak is also an indicator of the porous nature of the passivation layers, as when the electrolyte has a greater contact with the Al metal, the resistance naturally decreases.[18] In contrast, a totally insulating non-porous passivation layer would behave like a pure coating with a mostly capacitive behavior and hinder any signature of this interface.[19,20] Therefore, the resistance difference between **Cell 1** and **Cells 2–3** (20 kΩ and ≈150 kΩ, respectively) can be explained by the nature of the passivation layers (porosity and thickness). Amirudin et al.[21] similarly observed up to three orders of magnitude differences, and attributed this to heterogeneity of the coatings on the metal electrodes. Additionally, the rapid evolution of the spectra indicate transformations of the Al electrode/electrolyte interface, which, as pointed out by Elia et al.[22] are of largely unclear nature.

To further investigate the results obtained from PEIS, the spectra were fitted to ECs, for which the evolution of each element during OCV was tracked (**SI, Note 1**). An EC with three resistive elements corresponding to the electrolyte (R1), oxide-rich passivation layer (R2), and charge transfer (R4) resistance, and three capacitive elements assigned to the inorganic/organic (C1) and oxide-rich (CPE1) passivation layer and to the double layer (CPE2) capacitance, respectively, was found to provide the best description (Figs. S11a–12). In overall for **Cells 1–3** (Figs. S13–15), the oxide-rich passivation layer and Al electrode/passivation layers interface resistance and capacitance tend to increase, while the capacitance from the inorganic/organic passivation layer (C1) remains stable. These changes, suggest the growth of the oxide-rich passivation layer, which in turns renders the charge transfer process at the electrode/passivation layer interface more resistive. Additionally, it has been observed that the acidic nature of the ILE induces corrosion and dissolution of some of the species contained in the passivation layer or even the cell components.[14,23] Hence a simultaneous process of dissolution and redeposition of the passivation layers takes place and alters the morphology of these interfaces/layers, *e.g.* change in roughness.[4,18] Most of these changes happen at the oxide-rich layer while the inorganic/organic passivation layer is not subject to major changes and its thickness and roughness remain constant.

The SEM images show no drastic changes after OCV (**Cell 6–7**) as compared to the pristine Al (Figs. 1c–1d). The corresponding XPS Al2p spectra (Fig. 2) presents two peaks centered at 72.6 and ca.

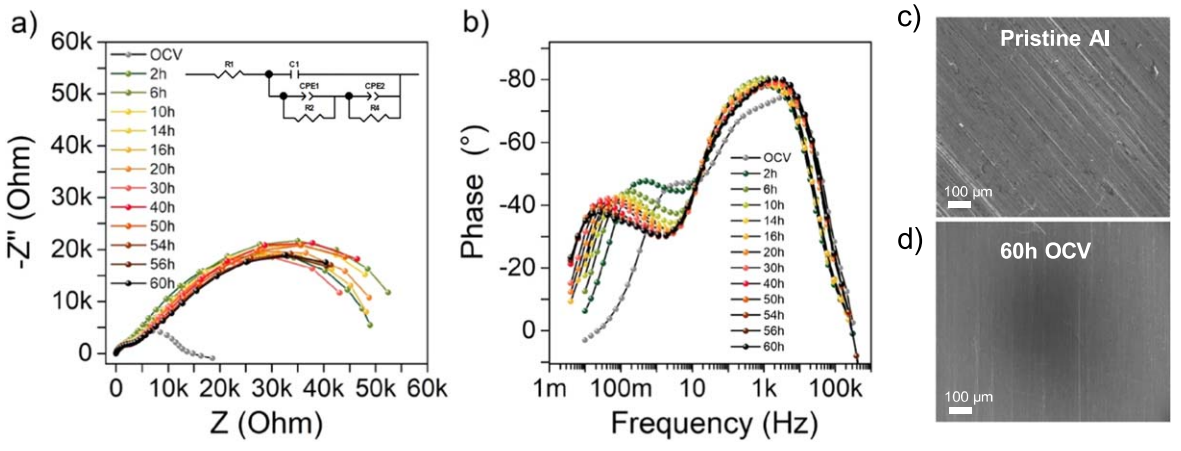

Figure 1. (a) Nyquist and (b) Bode plot for Cell 1 during an OCV period of 60 h. SEM images for (c) pristine Al foil and (d) Al-electrode after 60 h of OCV.

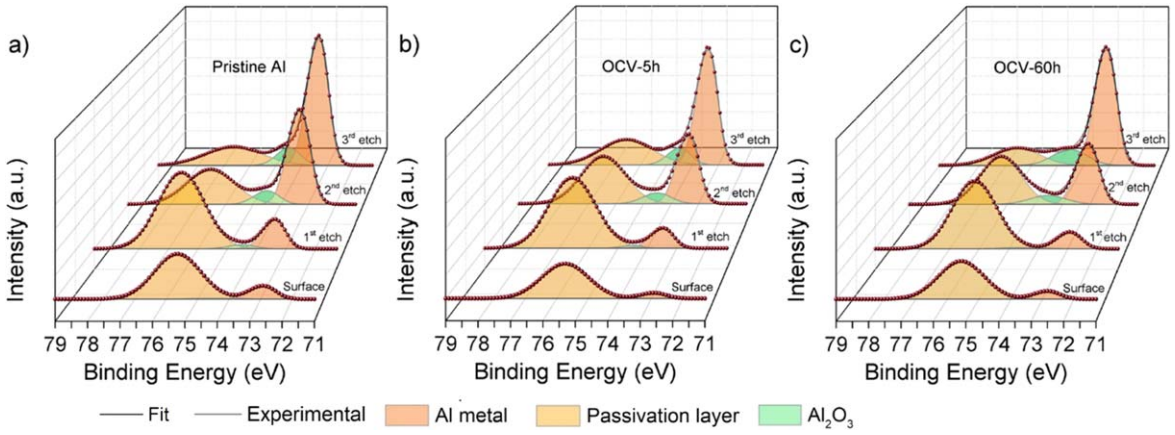

Figure 2. Al2p XPS spectra of (a) pristine Al electrode, and (b) **Cell 6** and (c) **Cell 7** after 5 and 60 h of OCV, respectively.

75–76 eV. The first we ascribe to metallic Al and the second to the passivation layers. After the first etching, the intensity of the former increases for all cases, due to removal of the passivation layers. The peak at 75 eV shifts to ≈76 eV and a new peak (green) emerges at *ca.* 74 eV. After the second and third etch and for all cases, the intensities of both the Al2p and new peak continue to increase, as more passivation layers have been removed, while the peak positions remain constant (**Table S1**). In more detail, the peak shifted to ≈76 eV in **Cells 6–7** is associated with the presence of halide bonds (74.5–76.3 eV), Al(AlO_x) (75.3–76.2 eV), and/or hydroxides (74.8–75.2 eV),[24] and hence mainly to inorganic/organic ILE decomposition products before the etchings and to oxides after the etchings.[24] The latter thus confirms the hypothesis of an outer passivation layer rich in inorganic/organic ILE decomposition products and an inner passivation layer rich in oxides. The peak at 74 eV may arise from the native Al_2O_3 (73.9–74.4 eV)[24] passivation layer, or from chemisorbed[25] or remaining oxygen in the vacuum chamber that can react with the newly exposed Al surface. It can also be an effect of the etching itself or other artefacts like atomic mixing, changes in the surface and bonding chemistry.[26] For the pristine Al electrode, never in contact with the ILE, the origin of both peaks at 76 and 74 eV might be different, *e.g.* hydroxides, ambient absorbed species (H_2O, CO_2), Al_2O_3 or several other types of oxides, with different Al-O coordination and signatures.[25] The pristine Al foil is thus not only metallic Al coated by alumina, but also other species exist.

In the O1s spectra (Fig. S21, SI Note 2) a single main peak at ≈533 eV is observed for all cases, but it has multiple variations (shift, intensity, shape) as function of both the OCV period and the etching. These changes are indicative of for instance Al-O (530–-531.8 eV), Al-OH_x (531–532 eV), C = O (532 eV), C-O (≈533 eV), O-Cl (532.6–533 eV) and O-N (532–533.5 eV)[24,27] and hence, multiple species may co-exist in the passivation layers (Table S1). After the first etch, the C content at the surface drops from 42–44 to <17 at% while the O content increases from 38–39 to >54 at%. After the second and third etch, however, the O content decreases. This is consistent with the presence of absorbed species at the surface of the pristine Al and with an outer inorganic/organic passivation layer, due to ILE decomposition for **Cells 6–7**, that are mostly removed after the first etch, leaving the oxygen-rich passivation layer more exposed. Upon subsequent etchings this layer is also removed and the Al metal contributions to the spectra become dominant.

The presence of carbonaceous species is supported by the C1s spectra (Fig. S21b, SI Note 2) with a main peak at *ca.* 285 eV (C-C bonds) which as before mainly arise from the outer surface and decrease upon etching (**Table S1**). This peak is due to the presence of carbonates formed by reaction of hydroxide species with ambient CO_2,[27] while after etching both oxides and ILE decomposition products passivation layer components co-exist: C-O, C-Cl, and C-N for **Cells 6–7** and different type of Al oxides are found in the pristine Al. Finally, in the Cl2p spectra a single peak is observed at ≈199 eV (Fig. S21c) and only at the surface of **Cells 6–7** and hence originate

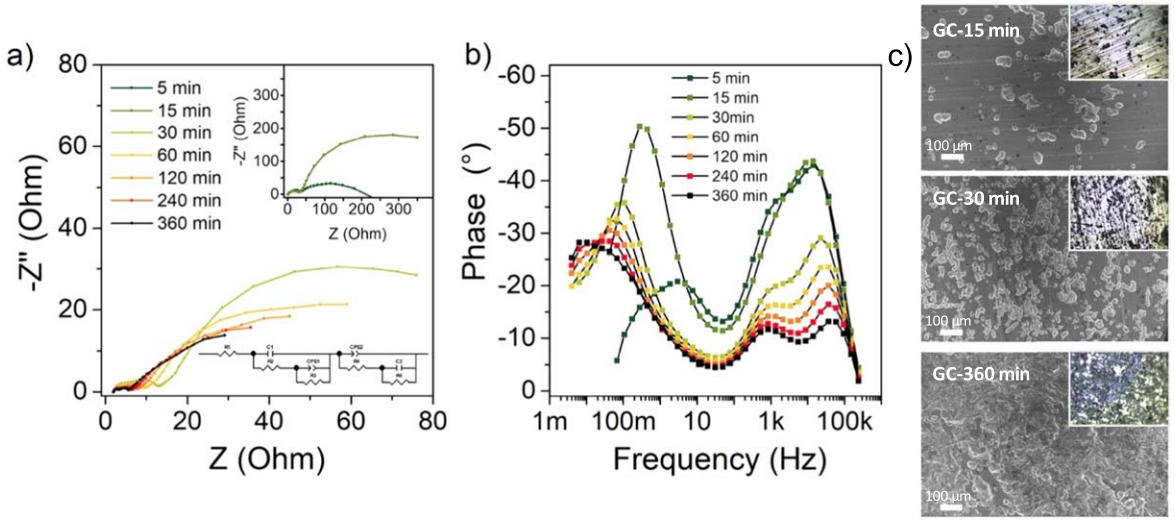

Figure 3. (a) Nyquist and (b) Bode plot for **Cell 1** after 5, 15, 30, 60, 120, 240 and 360 min of GC after an OCV period of 60 h. (c) SEM images after 15, 30 and 360 min of GC.

from ILE decomposition: Al-Cl (198.9–200.4 eV), Al-Cl-Al (199.4-–1997 eV), and Cl-organic (201.5–203.2 eV).[24,28]

In summary, the evolution of the passivation layers seems to be a complex process; due to the acidic ILE nature, some of the species must be dissolved, and at the same time the overall growth of principally the oxide-rich passivation layer implies that some of these species or ILE decomposition products are redeposited.[11,13–15,23] Overall the oxide-rich passivation layer tends to grow under OCV conditions, and as evidenced by the XPS data and supported by the EIS analysis, there is an outer passivation layer dominated by inorganic/organic oxides, carbonates, chlorides and nitrides, and an inner passivation layer which is oxide-rich.[4,11] Based on the XPS data, the thickness of both passivation layers was estimated to be 0.8 nm (see ***Note*3** in the SI).

Passivation layer formation during GC.—While the above analysis based on the Cells subjected to OCV conditions is important to understand battery functionality, the analysis of the Cells subjected to GC and any major changes between their behavior(s) bring another dimension to the understanding.

During the GC major changes were observed in the spectra; in the Nyquist plot, two semicircles can be detected, a small one at high frequency and a large one at low frequency (Fig. 3a). The interfacial resistances decrease from kΩ:s to a few hundred Ω, with most of the changes occurring within the first 5–30 min. This is a clear indicator of morphological changes taking place at the electrode, for instance a better contact between the Al metal and the electrolyte due to an increase in the porosity in the passivation layer. A relative larger resistance was found for the Cells with an OCV period (**Cells 1–3**) (Fig. S4–5) as compared to those without (**Cells 4–5**) (Fig. S6–7). This also shows in the Bode plot, by two peaks at high frequency and one at low frequency (Fig. 3b). In analogy to the OCV data, the first two represent two time-constants of similar magnitude, assigned to the inorganic/organic and oxide-rich passivation layers. These peaks become more defined during the GC, indicating changes in both passivation layers, e.g. increased ILE permeation, as characterized by a decrease in phase angle and resistance. In contrast, this was not observed during the OCV period when the ILE permeation was more limited.[29] The peak at low frequency is ascribed to the several modification processes at the Al metal/passivation layers interface, evidenced by the evolution of the peak shape and phase angle.

A different EC, as compared to the OCV analysis, was needed to describe the data during GC (SI, Note 1, Fig. S11b) with new elements ascribed to new interfaces. These are possibly the pits created by galvanic corrosion and/or the deposition of decomposition products inside them.[4] In total five resistive and four capacitive elements were used: the electrolyte (R1), inorganic/organic (R2) and oxide-rich (R3) passivation layers, charge transfer (R4) and pits/deposited products (R5) resistances, and the inorganic/organic (C1) and oxide-rich

(CPE1) passivation layers, double layer (CPE2) and pits/deposited products (C2) capacitances (Figs. S11–12, S16–20). The drastic reduction in the resistance as compared to the OCV data is associated with a higher overall porosity in both passivation layers,[21] likewise, the dispersion in the capacitances indicates a morphology evolution at the interfaces.[4,18] Both these evolutions possibly begin by the dissolution of the passivation layers through the pores, until reaching the Al electrode. As the metallic Al suffers from corrosion, the formation of primary and secondary pits happens, followed by unevenly deposition of Al in the freshly exposed areas, why the surface is re-structured. At the same time ILE decomposition products deposit inhomogeneously in the pits, into new or already existing surfaces, or accumulate in the pores.

The corrosion and pit formation can be observed in the SEM analysis, but also, after only 15 min of GC, even by optical microscopy (Fig. 3c). As the GC proceeds, the diameter of the pits increases and eventually interconnect until covering most of the surface (Figs. 3c, S8). When no OCV was performed prior the GC (**Cell 4,** Fig. S9), however, the pits seem to have a different morphology and after 360 min of GC they have a different size, rather sharper edges, and do not cover all the surface (Fig. S9c). Thus, the presence of thicker passivation layers (inorganic/organic and oxide-rich) formed under OCV conditions, seems to have an impact on the nucleation and formation of the pits.

In general, the degree of corrosion and pit formation seems to vary between Cells, in agreement with the dispersity in the resistances found by PEIS, and as this only was found during/after GC, it is electrochemically triggered.

From the XPS data, and in analogy to the OCV subjected Cells, the Al 2p spectra have two main peaks at the electrode surface at *ca.* 72.6 and 75–76 eV, the first ascribed to the Al metal and the second to the passivation layers (Figs. 4a-4b). After 360 min of GC (**Cell 9**), a third peak at 74 eV appears, which we assign to Al_2O_3. In analogy with our analysis above, the peak between 75–76 eV is the signature of both the outer inorganic/organic (oxides, carbonates, chlorides and nitrides) and the inner oxide-rich passivation layers. As the GC proceeds, the electrochemical etching of the passivation layers gradually exposes the Al metal, and the Al peak intensity increases

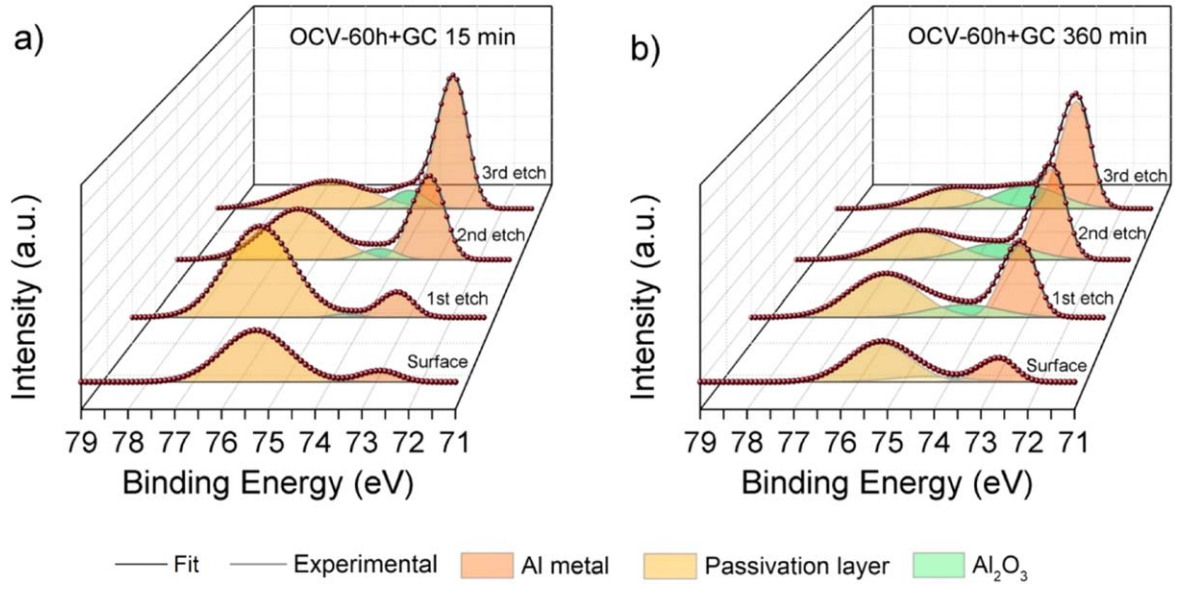

Figure 4. Al2p XPS spectra of an Al electrode for (a) **Cell 8** and (b) **Cell 9** after 60 h OCV + 15 and 360 min of GC, respectively.

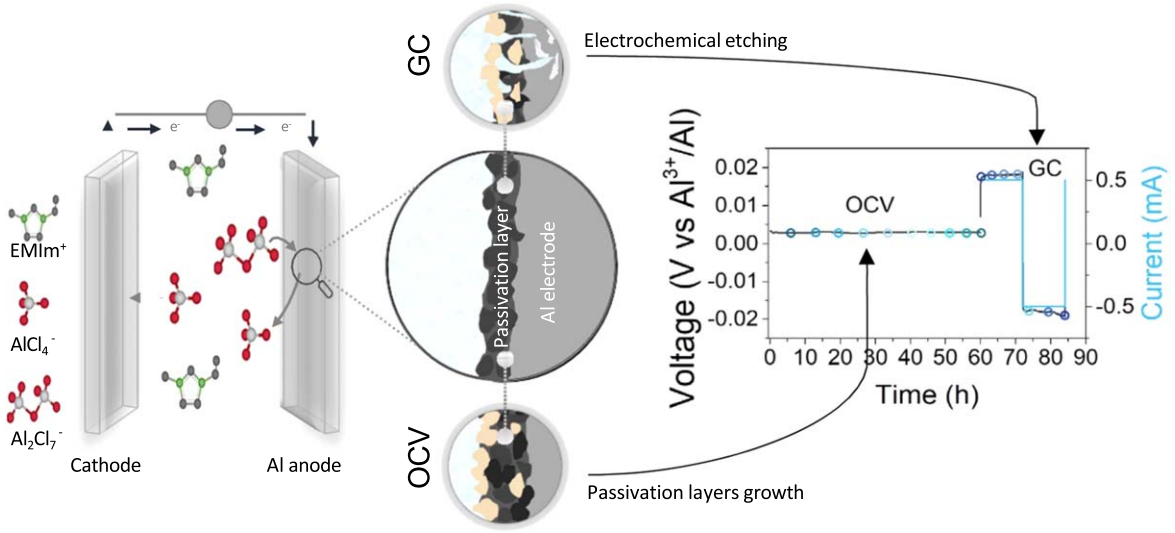

Figure 5. Schematic of processes taking place under OCV conditions and during GC.

(Figs. 4a-4b**, table S1**). After the etchings, both the peaks at 72.6 and 75–76 eV shift to higher binding energies, while the one at 74 eV remains constant, for both **Cells 8 and 9**.

In the O1s spectra (Fig. S22a), both **Cells 8** and **9** (15 and 360 min GC) render a single peak at ca. 532.9 eV, from O–C, –OH_x, O–Cl, or O–N bonds[24,27] present in the outer inorganic/organic passivation layer. After etching, the peak shifts to higher binding energies, likely due to the inner oxide rich passivation layer being detected (Table S1). The C1s spectra (Fig. S22b) is composed of a peak at ≈285.5 eV with a shoulder at ≈287 eV. The first can be assigned to C–O, C–Cl, C–N bonds and the second to decomposition products of the [EMIM]Cl in the ILE.[16,24,28] After the first etch, both these peaks decrease drastically in intensity, showing that the carbon-containing species are primarily located at the very outer surface (**Table S1**). Similarly, the Cl2p spectra (Fig. S22c), composed of a main peak at 199.3 eV, associated with Al-Cl, Al-Cl-Al or Cl-CO_x[28] also originate mainly from the very outer surface. The C and Cl total distributions are, however, inhomogeneous, with the species to be found over the entire depth of the passivation layers, as for instance with a content relatively higher for the first etch in **Cell 9** (360 min GC). We believe this to show that the electrochemical etching and the deposition of ILE decomposition products can change the distribution of the species over the probing depth and render very inhomogeneous passivation layers.

In summary, the GC induces severe structural modifications to the electrode as electrochemical etching takes place on the passivation layers and the Al metal, with partial dissolution and pit formation, respectively. The former creates pores that allow direct contact between the ILE and the Al metal, which modifies the interfacial resistance. In parallel, the ILE decomposition products are deposited on the passivation layer and/or in its pores or on freshly exposed Al surfaces. Overall, the passivation layers are found to be inhomogeneous with a tendency for ILE decomposition species (inorganic/organic) to be present at the surface and with oxides underneath, in line with the literature.[4,11,13–15,23]

Conclusions

The native oxide passivation layer at the Al metal surface has a very complex nature; its composition depends on the storing and production conditions,[30] e.g., temperature and humidity influence the absorption of other species such as water, hydroxides and carbon dioxide. Hence, multiple chemical species are present, rather than merely Al_2O_3. Our results indicate that once the AlB cells are assembled and the Al electrode is in contact with the ILE, two different types of passivation layers will be created: an outer inorganic/organic (carbonates, chlorides and nitrides) and an inner oxide rich. Both layers evolve with time, both under OCV conditions and during GC.

To outline the overall events, we present a schematic of the gained understanding of the processes occurring (Fig. 5). Under OCV conditions, due to ILE decomposition products depositing and side reactions, the passivation layers grow, and while they do offer some protection, they eventually corrode and dissolve,[13,15,23] leading to an intricate distribution of species and re-structuring of the electrode, e.g. change in porosity, affecting both the interfacial resistance and the diffusion of the electrolyte.

During the GC, the processes taking place are even more complex and the electrode is modified to a greater extent. The GC induces an electrochemical etching that not only attacks both passivation layers, exacerbating their dissolution, but also causes pit formation of the Al metal. The longer the GC, the greater the electrochemical etching. At the same time, the ILE decomposition products are deposited onto the freshly created surfaces or onto already existing ones. This continuous process of dissolution and deposition, along with the Al etching and plating/stripping, leads to unstable interfaces.[15] There has indeed been suggested that Al dendrites can nucleate in the pits or beneath the passivation layers.[13,14] When the passivation layers are pre-removed from the electrode, the Al metal suffers from excessive corrosion, uncontrolled dendrite growth, re-structuring, and integrity loss, hence the cyclability of the cells is compromised.[14,15,23] Therefore, the passivation layer plays an important role in ensuring the Al metal protection, preventing the electrode disintegration and excessive dendrite formation.[13,14] Nonetheless, a certain corrosion or porosity is needed to ensure the contact between the electrolyte and the Al metal, and enable the reversible redox reaction.[14,23]

With the insights gained from our work, we recommend the rational design of an ionic conducting protective film to allow the implementation of non-acidic non-aqueous electrolytes while granting the redox reaction. The implementation of such a strategy will possibly simplify the processes taking place at the interface (no electrochemical etching—less electrode restructuring) and facilitate the choice of cell components (no/less need for corrosion resistant materials). Alternatively, the design of an effective protection for the Al electrode from the acid ILE could lead to more stable interfaces that will extend the life cycle of the cells.

Acknowledgments

The authors are grateful for the financial support from the Swedish Energy Agency through grants #50121–1 and #43525–1.

ORCID

Laura C. Loaiza https://orcid.org/0000-0002-3164-4509
Patrik Johansson https://orcid.org/0000-0002-9907-117X

References

1. T. Leisegang, F. Meutzner, M. Zschornak, W. Münchgesang, R. Schmid, T. Nestler, R. A. Eremin, A. A. Kabanov, V. A. Blatov, and D. C. Meyer, *Front. Chem.*, **7**, 1 (2019).
2. B. Craig, T. Schoetz, A. Cruden, and C. Ponce de Leon, *Renew. Sustain. Energy Rev.*, **133**, 110100 (2020).
3. D. Muñoz-Torrero, M. Anderson, J. Palma, R. Marcilla, and E. Ventosa., *ChemElectroChem*, **6**, 2766 (2019).
4. T. Dong, K. L. Ng, Y. Wang, O. Voznyy, and G. Azimi, *Adv. Energy Mater.*, **11**, 1 (2021).
5. Q. Zhao, M. J. Zachman, W. I. Al Sadat, J. Zheng, L. F. Kourkoutis, and L. Archer., *Sci. Adv.*, **4**, 1 (2018).
6. P. R. Gifford and J. B. Palmisano., *J. Electrochem. Soc.*, **135**, 650 (1988).
7. K. V. Kravchyk and M. V. Kovalenko., *Commun. Chem.*, **3**, 1 (2020).
8. S. Das, S. S. Manna, and B. Pathak., *ACS Omega*, **6**, 1043 (2021).
9. M. C. Lin et al., *Nature*, **520**, 325 (2015).
10. K. V. Kravchyk, C. Seno, and M. V. Kovalenko., *ACS Energy Lett.*, **5**, 545 (2020).
11. T. Jiang, M. J. Chollier Brym, G. Dubé, A. Lasia, and G. M. Brisard, *Surf. Coatings Technol.*, **201**, 1 (2006).
12. S. Wang, K. V. Kravchyk, A. N. Filippin, U. Müller, A. N. Tiwari, S. Buecheler, M. I. Bodnarchuk, and M. V. Kovalenko., *Adv. Sci.*, **5**, 1 (2018).
13. Y. Long, H. Li, M. Ye, Z. Chen, Z. Wang, Y. Tao, Z. Weng, S. Z. Qiao, and Q. H. Yang, *Energy Storage Mater.*, **34**, 194 (2021).
14. H. Chen, H. Xu, B. Zheng, S. Wang, T. Huang, F. Guo, W. Gao, and C. Gao., *ACS Appl. Mater. Interfaces*, **9**, 22628 (2017).
15. D. Lee, G. Lee, and Y. Tak., *Nanotechnology*, **29**, 36LT01 (2018).
16. S. Kumar, V. Verma, H. Arora, W. Manalastas, and M. Srinivasan, *ACS Appl. Energy Mater.*, **3**, 8627 (2020).
17. H. Wang, S. Gu, Y. Bai, S. Chen, F. Wu, and C. Wu., *ACS Appl. Mater. Interfaces*, **8**, 27444 (2016).
18. R. Böttcher, S. Mai, A. Ispas, and A. Bund., *J. Electrochem. Soc.*, **167**, 102516 (2020).
19. F. Mansfeld., *Electrochim. Acta*, **35**, 1533 (1990).
20. H. Herrera Hernandez, A. M. Ruiz Reynoso, J. C. Trinidad Gonzalez, C. O. Gonzalez Moran, A. Miranda Hernandez, J. Jose Mandujano Ruiz, M. Hernandez, and R. Orozco Cruz, *Electrochemical Impedance Spectroscopy*, ed. M. El-Azazy, Vol. 32, p. 137 (2020).
21. A. Amirudin and D. Thieny., *Prog. Org. Coatings*, **26**, 1 (1995).
22. G. A. Elia, J. B. Ducros, D. Sotta, V. Delhorbe, A. Brun, K. Marquardt, and R. Hahn., *ACS Appl. Mater. Interfaces*, **9**, 38381 (2017).
23. S. Choi, H. Go, G. Lee, and Y. Tak., *Phys. Chem. Chem. Phys.*, **19**, 8653 (2017).
24. John F. Moulder, William F. Stickle, Peter E. Sobol, and Kenneth D Bomben, *Handbook of X-ray Photoelectron Spectroscopy*, ed. Jill Chastain (United States of America, Perkin-Elmer Coorporation) (1992).
25. C. Berg, S. Raaen, A. Borg, J. N. Andersen, E. Lundgren, and R. Nyholm., *Phys. Rev. B*, **47**, 13063 (1993).
26. G. Greczynski and L. Hultman, *Appl. Surf. Sci.*, **542**, 148599 (2021).
27. J. Zähr, S. Oswald, M. Türpe, H. J. Ullrich, and U. Füssel, *Vacuum*, **86**, 1216 (2012).
28. N. Canever, F. R. Hughson, and T. Nann, *ACS Appl. Energy Mater.*, **3**, 3673 (2020).
29. J. Wang, Z. Mi, H. Jiang, and R. Wang., *J. Mater. Sci.*, **54**, 6608 (2019).
30. M. Textor and M. Amstutz., *Anal. Chim. Acta*, **297**, 15 (1994).